

The SUMO-specific isopeptidase SENP2 is targeted to intracellular membranes via a predicted N-terminal amphipathic α -helix

Hana M. Odeh^a, Etienne Coyaud^b, Brian Raught^{b,c}, and Michael J. Matunis^{a,*}

^aDepartment of Biochemistry and Molecular Biology, Bloomberg School of Public Health, Johns Hopkins University, Baltimore, MD 21205; ^bPrincess Margaret Cancer Centre, University Health Network, Toronto, ON M5G 2C4, Canada; ^cDepartment of Medical Biophysics, University of Toronto, Toronto, ON M5G 1L7, Canada

ABSTRACT Sumoylation regulates a wide range of essential cellular functions, many of which are associated with activities in the nucleus. Although there is also emerging evidence for the involvement of the small ubiquitin-related modifier (SUMO) at intracellular membranes, the mechanisms by which sumoylation is regulated at membranes is largely unexplored. In this study, we report that the SUMO-specific isopeptidase, SENP2, uniquely associates with intracellular membranes. Using *in vivo* analyses and *in vitro* binding assays, we show that SENP2 is targeted to intracellular membranes via a predicted N-terminal amphipathic α -helix that promotes direct membrane binding. Furthermore, we demonstrate that SENP2 binding to intracellular membranes is regulated by interactions with the nuclear import receptor karyopherin- α . Consistent with membrane association, biotin identification (BioID) revealed interactions between SENP2 and endoplasmic reticulum, Golgi, and inner nuclear membrane-associated proteins. Collectively, our findings indicate that SENP2 binds to intracellular membranes where it interacts with membrane-associated proteins and has the potential to regulate their sumoylation and membrane-associated functions.

Monitoring Editor
Karsten Weis
ETH Zurich

Received: Jul 7, 2017
Revised: Apr 30, 2018
Accepted: Jun 1, 2018

INTRODUCTION

The small ubiquitin-related modifier (SUMO) is a highly conserved 100–amino acid protein that is posttranslationally and covalently attached to a multitude of other proteins (Wilson, 2017). Similarly to other ubiquitin-like proteins, sumoylation adds another level of regulation to protein activity, stability, and localization. Yeast and invertebrates express one SUMO protein, while vertebrates express several functional paralogues, including SUMO-1, SUMO-2, and SUMO-3. Mammalian SUMO-2 and SUMO-3 are 95% identical and thought to be functionally related. However, SUMO-1 is only 50%

identical to SUMO-2/3 and may have unique functions (Citro and Chiocca, 2013). The mechanism of SUMO conjugation is closely related to ubiquitin. In brief, a SUMO-activating enzyme (E1) is required for the ATP-dependent activation of SUMO, which is then transferred to SUMO-conjugating enzyme (E2) forming a thioester intermediate. Ultimately, SUMO is transferred to substrate proteins, in some cases through the action of E3 ligases, where its C-terminal glycine is covalently linked to the ϵ -amino group of lysine residues in the target protein forming an isopeptide linkage (Cappadocia and Lima, 2018). In addition to its action through covalent conjugation, SUMO can also interact noncovalently with downstream effector proteins that contain SUMO-interacting motifs (SIMs) (Hay, 2013).

A wide range of essential cellular functions are regulated by sumoylation, many of which are associated with activities in the nucleus, including transcription, chromatin remodeling, and DNA repair (Hendriks and Vertegeal, 2016). However, there is growing evidence for the involvement of SUMO in the cytoplasm, most notably at intracellular membranes (Wasik and Filippek, 2014). For example, SUMO plays an important role in regulating the dynamin-related GTPase Drp1, which mediates mitochondrial fission once recruited to the outer mitochondrial membrane (Anderson and Blackstone, 2013). The misregulation of Drp1 sumoylation subsequently affects

This article was published online ahead of print in MBoc in Press (<http://www.molbiolcell.org/cgi/doi/10.1091/mbc.E17-07-0445>) on June 6, 2018.

*Address correspondence to: Michael J. Matunis (mmatuni1@jhu.edu).

Abbreviations used: BioID, biotin identification; EMC, ER membrane protein complex; GFP, green fluorescent protein; Kap- α , karyopherin- α ; MBP, maltose-binding protein; NLS, nuclear localization signal; NPC, nuclear pore complex; PBS, phosphate-buffered saline; SAINT, significance analysis of interactomes; SENP, sentrin-specific protease; SUMO, small ubiquitin-related modifier.

© 2018 Odeh et al. This article is distributed by The American Society for Cell Biology under license from the author(s). Two months after publication it is available to the public under an Attribution–Noncommercial–Share Alike 3.0 Unported Creative Commons License (<http://creativecommons.org/licenses/by-nc-sa/3.0>).

“ASCB®,” “The American Society for Cell Biology®,” and “Molecular Biology of the Cell®” are registered trademarks of The American Society for Cell Biology.

mitochondrial division and is associated with brain ischemia (Fu *et al.*, 2014). Another important SUMO substrate at membranes is the cystic fibrosis transmembrane conductance regulator (CFTR). In normal conditions, this multidomain membrane protein resides in the plasma membrane. However, the most common mutant form of CFTR associated with cystic fibrosis contains a destabilizing phenylalanine deletion at position 508 ($\Delta F508$) that causes the protein to be degraded at the endoplasmic reticulum (ER) membrane (Meng *et al.*, 2017). The degradation of $\Delta F508$ is mediated by the ubiquitin-proteasome pathway but has also recently been shown to involve sumoylation (Gong *et al.*, 2016). Finally, sumoylation controls the activity of multiple ion channels, including Kv7 potassium channels in hippocampal neurons linked to epilepsy and sudden death (Qi *et al.*, 2014). Despite these and other rapidly expanding roles for sumoylation at membranes, what remains to be elucidated is how the sumoylation machinery itself is targeted to membranes to control the modification of these proteins.

To investigate SUMO regulation at membranes more closely, we have focused our attention on the SUMO deconjugation machinery. The dynamic and reversible nature of sumoylation depends on the action of a variety of SUMO-specific proteases that cleave the isopeptide bond formed between the C-terminus of SUMO and its substrates. SUMO proteases also mediate SUMO precursor maturation, hence indirectly affecting SUMO conjugation. To date, there are three families of structurally distinct SUMO proteases: the SENP (sentrin-specific protease) family, the Desi (deSUMOylating isopeptidase) family, and USPL1 (ubiquitin-specific peptidase-like protein 1) (Nayak and Muller, 2014). In mammalian cells, SENPs represent the largest family of SUMO proteases, with a total of six encoded SENPs (SEN1-3 and SEN5-7), all of which share a conserved C-terminal catalytic domain and variable N-terminal domains (Hickey *et al.*, 2012).

The subcellular localization of individual SENPs is determined by distinct targeting signals within their N-terminal domains. Consequently, each SENP exhibits a unique subcellular localization that is believed to affect function by determining accessibility to specific substrates. SENP2, for example, localizes to the nuclear pore complexes (NPCs) in interphase and to kinetochores in mitosis (Goeres *et al.*, 2011; Cubeñas-Potts *et al.*, 2013). SENP2 localization depends on multiple N-terminal targeting signals, including a Nup107-160 subcomplex binding domain and a bipartite nuclear localization signal (NLS) that facilitates interactions with karyopherins and FG-repeat nucleoporins. Disrupting these signals affects not only SENP2 localization but also its functions in regulating the sumoylation of kinetochore-associated proteins and chromosome segregation in mitosis (Itahana *et al.*, 2006; Goeres *et al.*, 2011; Cubeñas-Potts *et al.*, 2013).

In addition to its association with NPCs and kinetochores, there is also evidence supporting a role for SENP2 in regulating the sumoylation of membrane-associated proteins. First, SENP2 regulates the sumoylation of Drp1, hence playing a role in mitochondrial fission (Fu *et al.*, 2014). In addition, SENP2 has been implicated in controlling the sumoylation of the potassium channel Kv7.2 at the plasma membrane. More specifically, reduced expression of SENP2 in mice results in hyper-sumoylation of Kv7.2 in hippocampal neurons, leading to increased neuronal excitability, seizures, and sudden death (Qi *et al.*, 2014). Thus, SENP2 is linked to pathophysiological processes involving sumoylation at membranes. How SENP2 is specifically targeted to protein substrates at membranes, however, is unknown.

In this study, we discovered a new signal within SENP2 that specifies a unique subcellular localization to intracellular membranes. We

show that SENP2 has a predicted amphipathic α -helix at its extreme N-terminus that allows it to directly interact with membranes. We also present evidence that the binding of Kap- α to an adjacent NLS regulates membrane interaction. Consistent with these findings, we found using BioID that SENP2 interacts with a subset of ER, Golgi, and inner nuclear membrane-associated proteins. Together, our findings have identified SENP2 as a SUMO protease with the potential to regulate sumoylation at membranes.

RESULTS

SENP2 associates with NPCs and with the inner nuclear membrane

SENP2 has previously been shown to associate with NPCs, based on fluorescence microscopy and mass spectrometry-based identification of interacting proteins (Hang and Dasso, 2002; Zhang *et al.*, 2002; Goeres *et al.*, 2011). In addition to punctate NPC localization, however, we have also observed that SENP2 can be more generally detected as a continuous staining of the inner nuclear membrane (Figure 1). To explore this localization more closely, we transiently expressed SENP2 as green fluorescent protein (GFP) fusion protein (GFP-SENP2) in HeLa cells and examined the colocalization with either mAb414 (a NPC marker) or lamin B (an inner nuclear membrane marker). Consistent with previous findings, SENP2 colocalized with NPCs but even more closely colocalized with lamin B (Figure 1, A and B). We then compared the localization of SENP2 with that of SENP1, a second SUMO isopeptidase also associated with NPCs (Chow *et al.*, 2012; Cubeñas-Potts *et al.*, 2013). Transient cotransfection of GFP-SENP2 with mCherry-SENP1 showed that SENP2 and SENP1 have distinct localization patterns. SENP2 displayed a more continuous staining at the nuclear envelope, whereas SENP1 was detected as punctae resembling NPC staining (Figure 1C). These results revealed that SENP2 associates with NPCs and also with the inner nuclear membrane. To elucidate the molecular basis of SENP2 localization in greater detail, we further explored the signals that target it to the inner nuclear membrane.

The extreme N-terminus of SENP2 contains both NPC and membrane-targeting signals

SENP2 contains multiple N-terminal signals specifying localization, including two signals that mediate interactions with NPCs. One signal within amino acids 1–63 consists of a bipartite NLS that mediates interactions with FG repeat nucleoporins through high-affinity karyopherin binding. A second signal, within amino acids 143–350, interacts with the Nup107-160 subcomplex of the NPC (Goeres *et al.*, 2011). To determine whether one or the other of these signals also directs SENP2 to the inner nuclear membrane, we closely examined the localization of GFP-tagged fusion proteins (Figure 2). GFP-SENP2(1-63) showed a continuous staining of the inner nuclear membrane similar to full-length SENP2 (Figure 2, A and B). In contrast, GFP-SENP2(143-350) showed a punctate pattern similar to NPC staining (Figure 2C). This result suggested that the first 63 amino acids of SENP2, in addition to promoting interactions with FG-repeat nucleoporins, might also have an additional signal that facilitates associations with the inner nuclear membrane. To explore this prediction, we deleted the first nine amino acids and analyzed the localization of GFP-SENP2(10-63) (Figure 2D). Consistent with the presence of a second, membrane targeting signal, GFP-SENP2(10-63) was no longer concentrated at the nuclear periphery but instead showed a diffuse nucleoplasmic localization. Thus, the extreme N-terminus of SENP2 contains both NPC and inner nuclear membrane targeting signals.

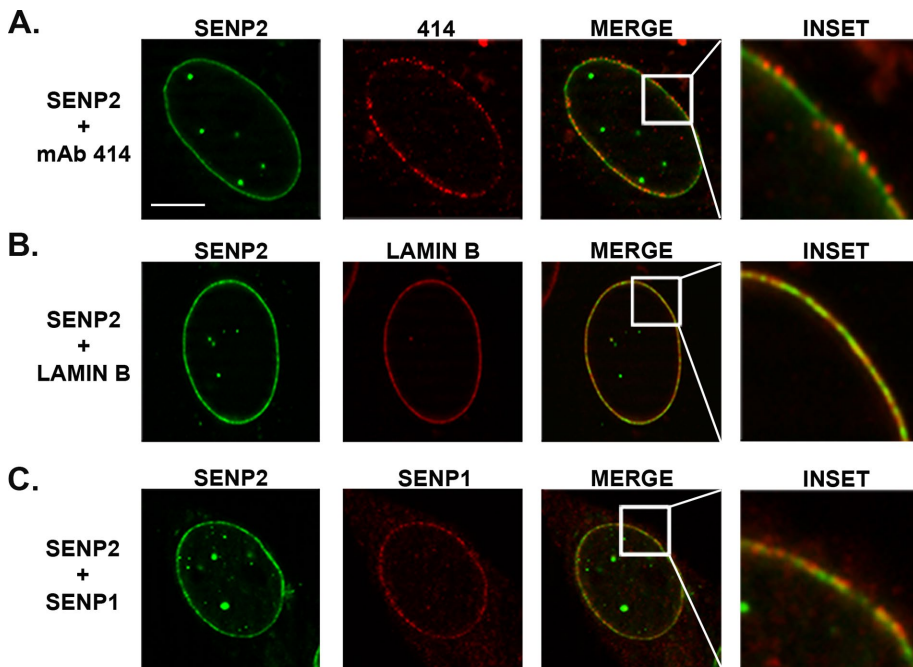


FIGURE 1: SENP2 localizes to NPCs and the inner nuclear membrane. HeLa cells were transiently transfected with full-length GFP-SENP2, and colocalization with NPCs, nuclear lamina, or mCherry-SENP1 was assessed by fluorescence microscopy. (A) Cells were stained with mAb 414, an antibody specific for nucleoporins. GFP-SENP2 partially colocalized with the punctate NPC staining. (B) Cells were stained with an antibody specific for lamin B, a marker for the inner nuclear membrane. GFP-SENP2 colocalized with the continuous lamin B nuclear rim staining. (C) Cells were cotransfected with mCherry-SENP1. SENP1 and SENP2 colocalized at NPCs. Continuous rim staining and localization to the inner nuclear membrane is unique to SENP2. Scale bar = 5 μ m.

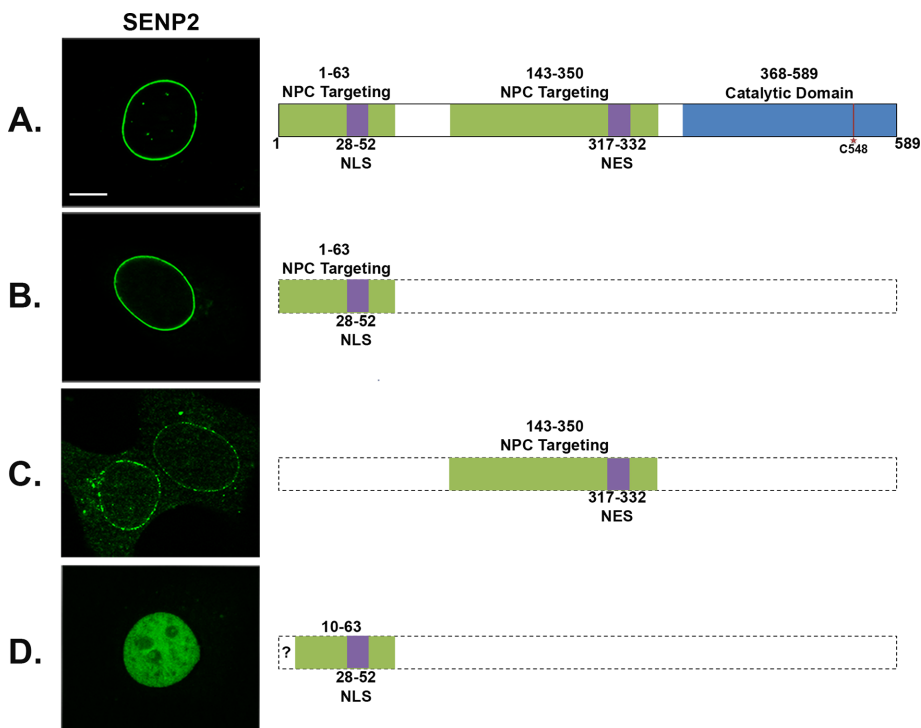


FIGURE 2: The extreme N-terminus of SENP2 directs localization to the inner nuclear membrane. HeLa cells were transiently transfected with full-length GFP-SENP2 or the indicated SENP2 deletion constructs and analyzed by fluorescence microscopy. (A) GFP-SENP2 localizes to NPCs and the inner nuclear membrane. (B) GFP-SENP2(1-63), containing a bipartite NLS, localizes to NPCs and the inner nuclear membrane similarly to full-length SENP2. (C) GFP-SENP2(143-350), containing a nuclear export signal (NES) and a signal that binds the Nup107-160 subcomplex of the NPC, localizes only to NPCs. (D) GFP-SENP2(10-63) localizes to the nucleoplasm, suggesting the presence of an extreme N-terminal signal that targets SENP2 to the inner nuclear membrane. Scale bar = 5 μ m.

The extreme N-terminus of SENP2 contains a predicted amphipathic α -helix

To explore how residues in the extreme N-terminus of SENP2 may function in targeting to the inner nuclear membrane, we performed secondary structure analysis and identified a predicted amphipathic α -helix that could serve as an in-plane membrane anchor (Figure 3, A and D). Sequence alignment of the first 52 amino acids of SENP2 demonstrated that the predicted amphipathic α -helix is highly conserved within mammals (Figure 3B). Interestingly, although the extreme N-terminus of zebrafish SENP2 is not conserved at the amino acid sequence level with mammalian SENPs, it nonetheless contains a predicted amphipathic α -helix (Figure 3C). This suggests that the predicted amphipathic α -helix has an essential role in the overall function of SENP2.

To test whether the targeting of SENP2 to the inner nuclear membrane is dependent on this predicted amphipathic α -helix, we generated a mutant GFP-SENP2 expression construct with isoleucine 8 mutated to aspartic acid (I8D) in the hydrophobic face of the predicted amphipathic α -helix (Figure 3D). Wild type or I8D mutant GFP-SENP2 proteins were transiently expressed in HeLa cells and their localization analyzed using fluorescence microscopy. Compared to wild-type SENP2, the I8D mutant showed reduced targeting to the inner nuclear membrane and enhanced nucleoplasmic localization (Figure 3E, top panel). The SENP2 I8D mutant retains the 143-350 NPC targeting signal, explaining the observed residual membrane localization. To more clearly assess the ability of the predicted amphipathic α -helix to target SENP2 to the inner nuclear membrane, we evaluated the localization of wild-type and I8D mutant GFP-SENP2(1-63). In contrast to wild-type GFP-SENP2(1-63), the I8D mutant showed only diffuse nucleoplasmic localization comparable to that observed with GFP-SENP2(10-63) (Figures 3E and 2D). These results are consistent with the predicted N-terminal amphipathic α -helix acting as an in-plane membrane

localizes to NPCs and the inner nuclear membrane similarly to full-length SENP2. (C) GFP-SENP2(143-350), containing a nuclear export signal (NES) and a signal that binds the Nup107-160 subcomplex of the NPC, localizes only to NPCs. (D) GFP-SENP2(10-63) localizes to the nucleoplasm, suggesting the presence of an extreme N-terminal signal that targets SENP2 to the inner nuclear membrane. Scale bar = 5 μ m.

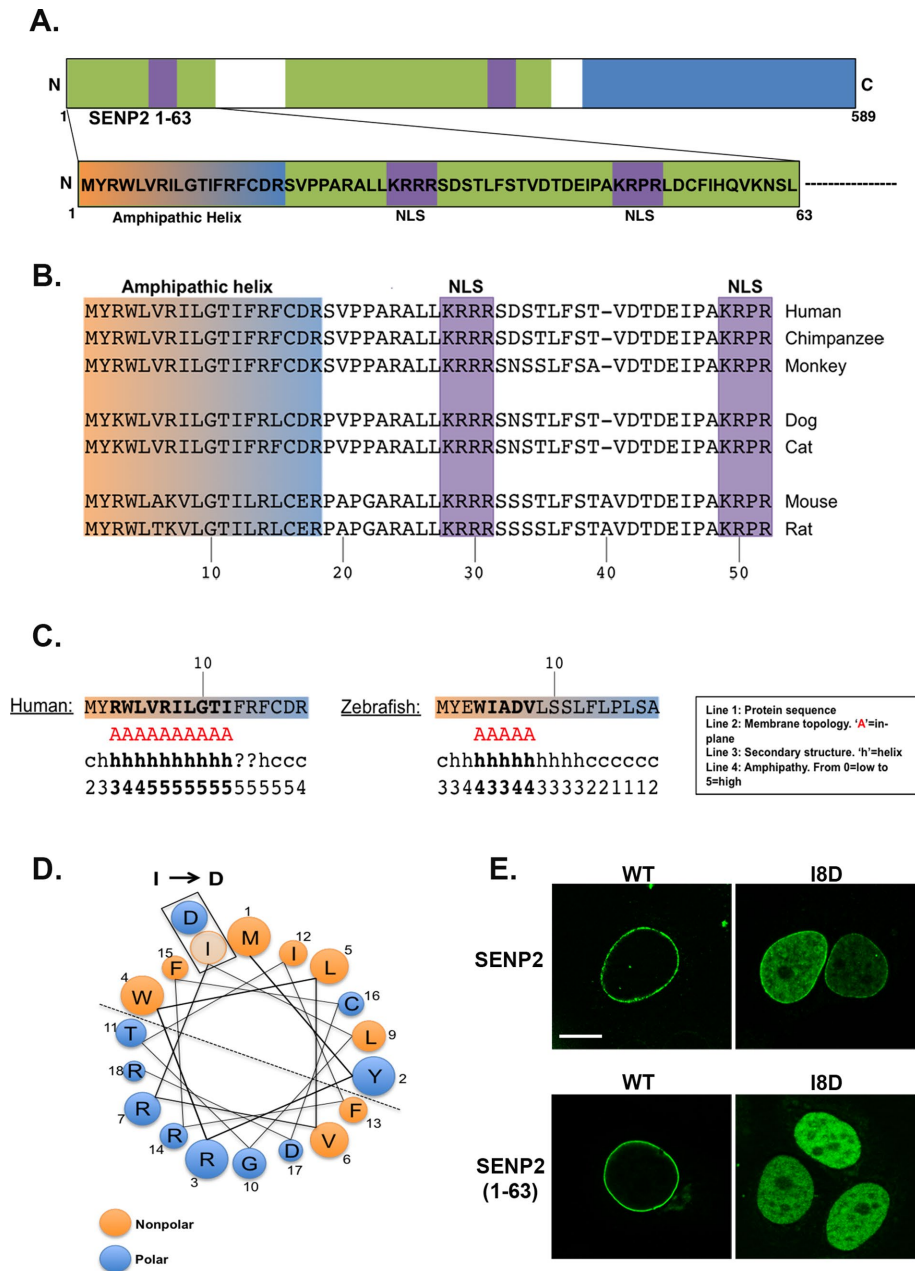


FIGURE 3: SENP2 has a predicted amphipathic α -helix at the extreme N-terminus. (A) Schematic diagram of full-length SENP2. Sequence and structure prediction analyses of the first 63 amino acids revealed that SENP2 has a predicted N-terminal amphipathic α -helix, highlighted in orange and blue. Analysis was performed using the AmphipaseE prediction method (Sapay *et al.*, 2006). (B) Sequence alignment of the first 52 amino acids of SENP2. The sequence of the predicted amphipathic α -helix is highly conserved among mammals. (C) Amphipathic in-plane membrane anchor predictions of SENP2 in human and zebrafish. Lines 1 through 4 show the first 18-amino acid sequence of SENP2, membrane topology, secondary structure, and level of amphipathy, respectively. Although not conserved at the sequence level, human and zebrafish SENP2 share a predicted amphipathic α -helix at the extreme N-terminus. (D) Helical wheel representation of the predicted amphipathic α -helix. Orange indicates nonpolar residues, and blue indicates polar residues. The position of the isoleucine 8 to aspartic acid substitution (I8D) is indicated. (E) HeLa cells were transiently transfected with wild-type (WT) GFP-SENP2, GFP-SENP2(1-63), or the equivalent I8D mutants and analyzed by fluorescence microscopy. The I8D mutation resulted in a diffuse nucleoplasmic localization and reduced membrane targeting, suggesting that the predicted amphipathic α -helix serves as in-plane membrane anchor that tethers SENP2 to the inner nuclear membrane. Scale bar = 5 μ m.

anchor that tethers SENP2 to the inner nuclear membrane.

Overproduction of SENP2 induces the formation of intranuclear membranes

In addition to localization at the nuclear membrane, GFP-SENP2 is also detected in intranuclear foci, whose number and intensity correlate with levels of SENP2 expression (Figure 1). Notably, the amphipathic α -helices of several other proteins, including Nup153 and Nbp1, form membranous intranuclear inclusions upon overexpression (Bastos *et al.*, 1996; Kupke *et al.*, 2011). To investigate whether GFP-SENP2 overexpression also induces the formation of intranuclear membranes, we performed immunoelectron microscopy on ultrathin cryosections of transfected HeLa cells (Figure 4). We found that intranuclear labeling was concentrated within densely stained inclusions containing membranous structures reminiscent of those detected in cells overexpressing the amphipathic α -helix of Nup153. Cells expressing GFP-SENP2^{I8D} did not show similar membranous structures (Supplemental Figure 1). These results are consistent with interactions between SENP2 and the inner nuclear membrane and suggest an ability to stimulate membrane formation.

The N-terminal amphipathic α -helix of SENP2 mediates direct membrane binding

Although predicted to interact directly with membranes, the N-terminus of SENP2 may also promote indirect binding to the inner nuclear membrane through interactions with other membrane-associated proteins. To test for direct membrane interaction, we expressed and purified recombinant wild-type and I8D mutant SENP2(1-63) as maltose binding protein (MBP) fusion proteins. The purified proteins were incubated with *in vitro* synthesized liposomes, and membrane binding was evaluated using a cosedimentation assay. Wild-type MBP-SENP2(1-63)^{WT} cosedimented with liposomes in a dose-dependent manner, consistent with direct membrane binding (Figure 5, A and C). In contrast, the I8D mutant MBP-SENP2(1-63)^{I8D} did not pellet with liposomes, revealing an essential role for the amphipathic α -helix in membrane binding (Figure 5, A and C). As a negative control, liposomes were incubated with purified recombinant MBP, which showed no direct membrane interaction (Figure 5A). As an additional control, recombinant proteins failed to sediment in the absence of liposomes (Figure 5B). Thus, our

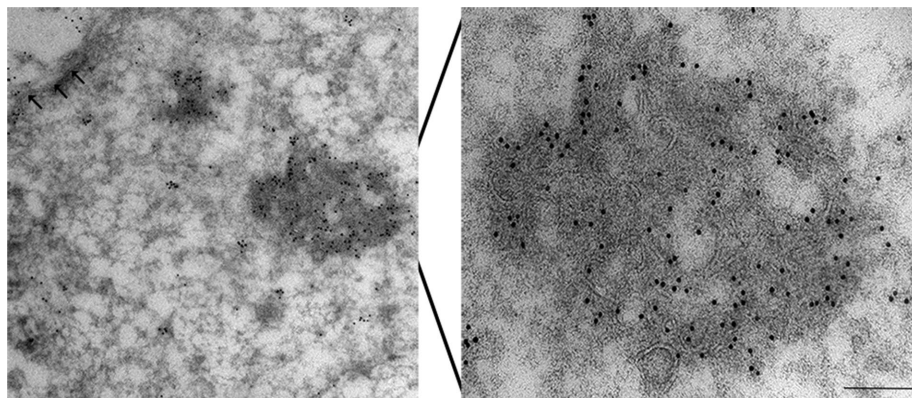


FIGURE 4: SEN2 overexpression results in the formation of intranuclear membrane arrays. HeLa cells were transiently transfected with full-length GFP-SEN2 and analyzed by immunoelectron microscopy using anti-GFP antibody. Micrographs reveal the presence of intranuclear membrane array upon SEN2 overexpression. Arrows indicate the inner nuclear membrane. Scale bar = 200 nm.

results demonstrate that the predicted N-terminal amphipathic α -helix of SEN2 binds directly to membranes.

SEN2 interactions with membranes can be modulated by Kap- α binding

SEN2 contains a bipartite NLS in close proximity to the predicted N-terminal amphipathic α -helix. This NLS binds with high affinity to

Kap- α and mediates its import to the nucleus and association with FG-repeat nucleoporins (Goeres *et al.*, 2011). Studies of other nuclear proteins containing N-terminal amphipathic α -helices in close proximity to functional NLSs, including Nbp1, Pom33, and Nup153, have found that karyopherin binding inhibits interactions with cytoplasmic membranes prior to delivery to the nucleus (Kupke *et al.*, 2011; Floch *et al.*, 2015; Vollmer *et al.*, 2015). To investigate whether Kap- α binding similarly controls the membrane interactions of SEN2, we performed liposome binding assays in the presence or absence of recombinant purified Kap- α . MBP-SEN2(1-63) alone, or in a 1:1 complex with Kap- α -6xHis (Figure 6D) was incubated in the presence or absence of membranes and sedimentation was evaluated by centrifugation. As previously observed, ~80% of MBP-SEN2(1-63) cosedimented with liposomes. In contrast, liposome binding of MBP-SEN2(1-63) was reduced by >50% in the presence of Kap- α and only ~10% of Kap- α itself associated with the liposome pellet (Figure 6, A and C). Because Kap- α alone has limited membrane affinity (Supplemental Figure 2), its membrane association in these experiments likely represents levels of MBP-SEN2(1-63)-Kap- α complexes bound to liposomes. Therefore, levels of Kap- α binding may more closely reflect its effects on MBP-SEN2(1-63) membrane interaction. Thus, our results reveal that SEN2 membrane interaction can be regulated by Kap- α binding. Next, we wanted to investigate Kap- α regulation in an *in vivo* setting.

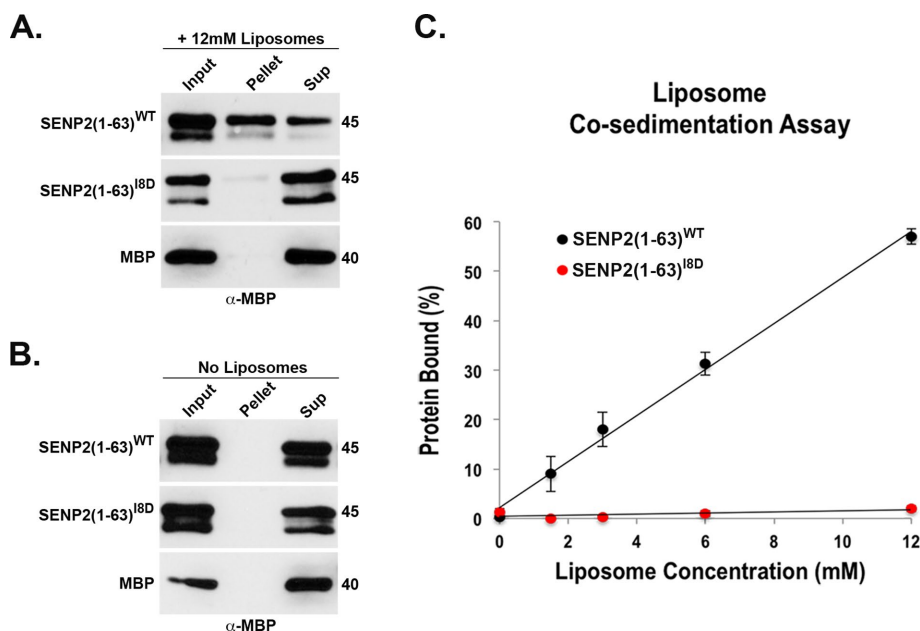


FIGURE 5: The N-terminus of SEN2 interacts directly with membranes. (A) Recombinant MBP-SEN2(1-63)^{WT} or MBP-SEN2(1-63)^{I8D} were incubated with liposomes and membrane binding was evaluated using a cosedimentation assay. Input, pellet, and supernatant fractions were analyzed by SDS-PAGE and immunoblotting using an anti-MBP antibody. MBP-SEN2(1-63)^{WT} cosedimented with liposomes, whereas the I8D mutant and MBP alone did not. (B) Control sedimentation assays were performed in the absence of liposomes. Proteins were only detected in the soluble fractions. (C) Quantitative analysis from three independent cosedimentation experiments performed in the presence of increasing concentrations of liposomes. MBP-SEN2(1-63)^{WT} bound to liposomes in a dose-dependent manner, whereas the I8D mutant showed negligible binding even at high liposome concentrations. Error bars indicate standard deviations from three independent experiments.

Disrupting the SEN2 N-terminal NLS facilitates targeting to cytoplasmic membranes

To investigate the effect of Kap- α binding on SEN2 localization *in vivo*, we analyzed the localization of a mutant GFP-SEN2(1-63) in which the NLS had been mutated at two residues (mNLS: R29A/R49A), thereby disrupting the Kap- α interaction (Goeres *et al.*, 2011). The effect of this NLS mutation on localization was first analyzed by fluorescence microscopy. In contrast to the nuclear membrane localization of GFP-SEN2(1-63), the NLS mutant protein showed a reticular-like staining pattern in the cytoplasm that partially colocalized with the ER marker, calnexin, and colocalized with the Golgi marker GM130 (Figure 7A). To further verify membrane localization in the cytoplasm, we isolated a fraction enriched for ER membranes by sucrose gradient sedimentation and performed immunoblot analysis. Consistent with the calnexin colocalization, GFP-SEN2(1-63)^{mNLS} was detected in the membrane fraction together with calnexin (Figure 7B, left panel). In contrast, when we combined the I8D and NLS mutations and performed the same fractionation analysis,

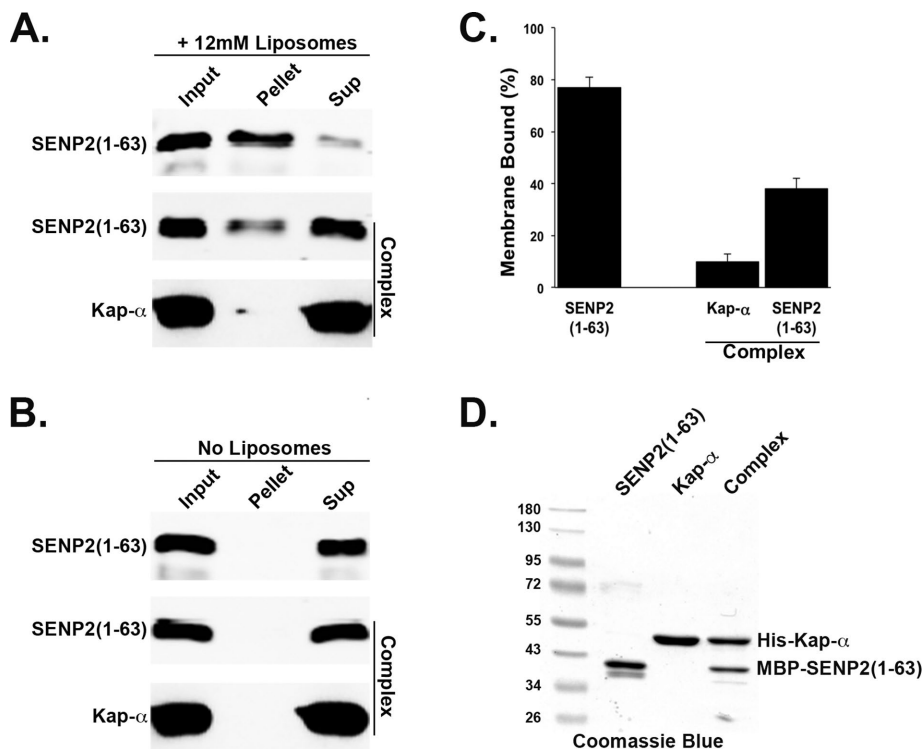


FIGURE 6: SENP2-membrane interaction is inhibited by Kap- α . (A) Recombinant MBP-SENP2(1-63) alone or in a 1:1 complex with Kap- α -6xHis was incubated with liposomes and membrane binding was evaluated using a cosedimentation assay. Input, pellet, and supernatant fractions were analyzed by SDS-PAGE and immunoblotting using anti-MBP and anti-His antibodies. When complexed with Kap- α , SENP2(1-63) membrane binding was inhibited. (B) Control sedimentation assays were performed in the absence of liposomes. (C) Quantification of SENP2(1-63) liposome binding alone or in the presence of Kap- α . Error bars indicate standard deviations from three independent experiments. (D) SDS-PAGE analysis of purified proteins and protein complexes used in the liposome cosedimentation assays.

we found that GFP-SENP2(1-63)^{mNLS/18D} was dramatically reduced in the membrane fraction and was mostly found in the soluble fraction with tubulin (Figure 7B, right panel). Our findings show that the N-terminus of SENP2 has the ability to associate with intracellular membranes in the cytoplasm, and this association is negatively regulated by Kap- α binding.

Endogenous SENP2 isoforms associate with intracellular membranes

Immunoblot analysis of endogenous SENP2 expressed in cultured mammalian cells reveals multiple isoforms ranging from 55 to 27 kDa that are thought to be derived through alternative splicing. Moreover, endogenous SENP2 is detected at the nuclear envelope but also in the nucleus and cytoplasm by immunofluorescence microscopy, suggesting differential localization of these isoforms (Goeres *et al.*, 2011). To explore possible associations of endogenous SENP2 with membranes, HeLa cells were fixed, permeabilized with digitonin, and then colabeled with antibodies recognizing SENP2 and the ER protein marker, GRP78 (Figure 8A). Consistent with ER membrane association, the cytoplasmic SENP2 signal colocalized with GRP78. To further validate this finding, we again isolated a fraction enriched for ER membranes by sucrose gradient sedimentation and performed immunoblot analysis (Figure 8B). Multiple SENP2 isoforms migrating at 50, 40, and 27 kDa copurified with the membrane fraction. However, one isoform migrating at ~48 kDa was uniquely detected in the soluble fraction. This isoform may corre-

spond to a splice variant identified in mice that lacks the 50 N-terminal amino acids, including the predicted amphipathic α -helix (Figure 8C) (Nishida *et al.*, 2001). To investigate whether the copurification of endogenous SENP2 isoforms with membranes may be due to interactions with NPCs, we probed fractions with mAb414, which recognizes multiple nucleoporins (Figure 8D). Nup358, Nup214, and Nup153 largely copurified with the soluble fraction, whereas p62 showed an equal distribution between soluble and membrane fractions. Thus, although it is unlikely that membrane interaction is due to binding to NPC filament proteins, NPC binding in general cannot be ruled out.

SENP2 interacts with membrane-associated proteins

Our results thus far provide evidence that SENP2 associates with the inner nuclear membrane, ER, and Golgi membranes. However, the sumoylated proteins regulated by SENP2 at these membranes remain largely unknown. We previously used an affinity purification–mass spectrometry (AP-MS)-based approach to isolate stable SENP2-interacting proteins and identified proteins of the nuclear pore complex (nucleoporins) and soluble nuclear transport receptors (Goeres *et al.*, 2011). To identify more transiently associated or less abundant SENP2-interacting proteins, including potential substrates, we turned to the proximity-dependent biotin identification (BioID) approach (Roux *et al.*, 2013). Stable cell lines for inducible expression of full-length wild-type SENP2 fused to the biotin ligase variant, BirA*, or the BirA* ligase alone were generated. Expression levels and localization of FLAG-BirA*-SENP2 were compared with endogenous SENP2 via immunofluorescence microscopy and immunoblot analysis (Supplemental Figure 3). Following induction, cells were cultured in the presence of biotin for 24 h and biotinylated proteins were purified by streptavidin affinity chromatography and analyzed by mass spectrometry (a full list of identified proteins is presented in Supplemental Table 3). This list of proteins was analyzed using the significance analysis of interactomes (SAINT) approach to identify high-confidence SENP2-interacting partners (Choi *et al.*, 2012). Consistent with previous AP-MS analysis (Goeres *et al.*, 2011), NPC-associated proteins were detected (Figure 9A and Supplemental Table 1). Of particular interest, and consistent with immunofluorescence microscopy, subcellular fractionation, and *in vitro* binding results, we also detected interactions with proteins of the inner nuclear membrane, ER, and Golgi that were not previously identified (Figure 9A and Supplemental Table 1). To test whether these unique interactions with SENP2 are dependent on its predicted amphipathic α -helix, we performed the BioID analysis using stably expressed FLAG-BirA*-SENP2^{18D}. Similarly to the wild-type SENP2, SENP2^{18D} interacted with NPC-associated proteins (Figure 9B), indicating that these interactions are independent on SENP2-membrane association. However, the SENP2^{18D} mutant lost association with most of the membrane-associated proteins compared with the wild-type

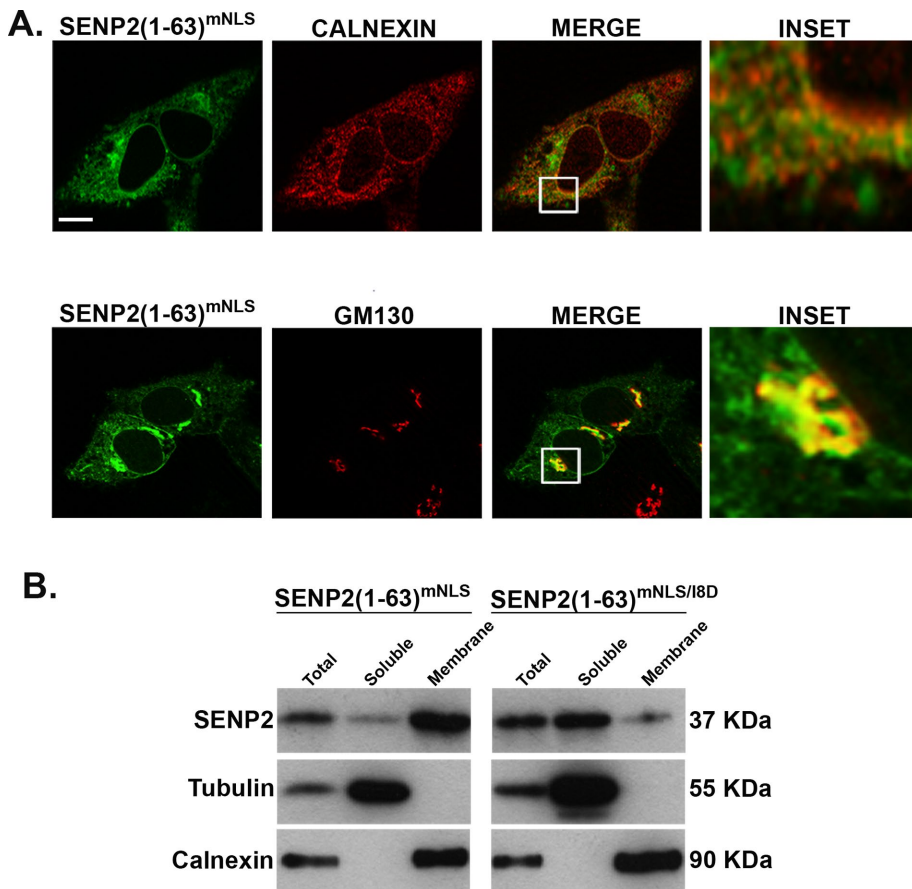


FIGURE 7: Disrupting the SENP2 N-terminal NLS enables targeting to ER and Golgi membranes. Using site-directed mutagenesis, alanine substitutions were generated at positions R29 and R49 within the SENP2 N-terminal NLS (designated mNLS) in both wild-type and I8D GFP-SENP2(1-63) expression constructs. (A) HeLa cells were transfected with GFP-SENP2(1-63)^{mNLS} and analyzed by indirect immunofluorescence microscopy. Cells were either stained using an anti-calnexin antibody (top panel) or an anti-GM130 antibody (bottom panel) to label ER and Golgi membranes, respectively. GFP-SENP2(1-63)^{mNLS} partially colocalized with calnexin and colocalized with GM130. Scale bar = 5 μ m. (B) HeLa cells were transfected with wild-type and I8D mutant GFP-SENP2(1-63)^{mNLS} and fractions enriched in ER membranes were isolated using sucrose gradient sedimentation. Soluble and membrane fractions were analyzed by immunoblotting. Tubulin and calnexin were detected as markers for soluble and membrane fractions, respectively. GFP-SENP2(1-63)^{mNLS} was concentrated in the membrane fraction, whereas GFP-SENP2(1-63)^{mNLS/I8D} was predominantly soluble.

protein, consistent with the N-terminal predicted amphipathic α -helix being responsible for SENP2-membrane binding (Figure 9B and Supplemental Table 1). Given the diffuse nucleoplasmic localization of SENP2^{I8D}, the mutant protein also gained new interactions with soluble nuclear proteins that did not interact with SENP2^{WT}.

DISCUSSION

As the functions of SUMO rapidly expand beyond the nucleus, evidence for SUMO regulation at multiple intracellular membranes continues to emerge. However, very little is known about how SUMO is affecting membrane-associated functions or how sumoylation is regulated at membranes. In this study, we have identified a novel interaction between SENP2, an essential regulator of SUMO dynamics, and intracellular membranes. We showed that SENP2 has a unique N-terminal amphipathic α -helix, absent in other SUMO proteases, which allows it to directly interact with membranes under the regulation of Kap- α . We also identified a unique

subset of membrane-associated proteins that interact with SENP2, providing further insights into the potential roles SUMO can play in regulating membrane-associated functions.

SENP2 predicted amphipathic α -helix and membrane interaction

Our previous study showed that SENP2 associates dynamically with NPCs (Goeres *et al.*, 2011). However, our immunofluorescence microscopy data reported here indicate that SENP2 not only associates with NPCs but also colocalizes with the inner nuclear membrane. Apparent differences in localization could be explained by GFP-SENP2 expression levels. At low expression levels, GFP-SENP2 showed punctate staining, closely resembling NPC staining. In contrast, the signal for moderate to high expression levels of GFP-SENP2 revealed localization to both the NPCs and the nuclear membrane (Supplemental Figure 4). Thus, SENP2 may have higher affinity for NPCs compared with the inner nuclear membrane itself. However, endogenous SENP2 localizes to membranes, including ER and Golgi, evident from subcellular fractionation and colocalization with GRP78. We performed colocalization studies with various Golgi marker proteins and endogenous SENP2 but were unable to detect obvious Golgi enrichment due to either the low level of SENP2 expression or transient interactions between SENP2 and Golgi-associated proteins and membranes. Nevertheless, consistent with membrane localization, in our BioID analysis we identified membrane-associated proteins that interact with SENP2 giving us further reason to explore this newly discovered SENP2-membrane interaction.

Sequence analysis and secondary structural predictions revealed that SENP2 has a unique N-terminal amphipathic α -helix, absent in other SUMO proteases. Our *in vivo* and *in vitro* analyses further demonstrated that this predicted amphipathic α -helix directly associates with membranes. Studies have shown that there are two classes of amphipathic α -helices, one that senses membrane curvature and one that induces membrane curvature (Drin and Antony, 2010). For instance, proteins with the ArfGAP1 lipid-packing sensor-like (ALPS) motif, composed of polar, uncharged residues, mainly serine and threonine, are more suitable for sensing membrane curvature (Drin *et al.*, 2007). Examples include the Golgi protein golgin GMAP-210 (Drin *et al.*, 2007) and nucleoporin Nup133 (Drin *et al.*, 2007). In contrast, amphipathic α -helices with basic, charged residues are thought to induce membrane curvature. Given that SENP2 has a stretch of basic, charged residues (refer to Figure 3D), we predict that its amphipathic α -helix is more suitable for inducing membrane curvature; however, further investigation is still required. Notably, multiple NPC-associated proteins with ALPS-like motifs (Nup120, Nup85, Nup170, and Nup188) or with a basic

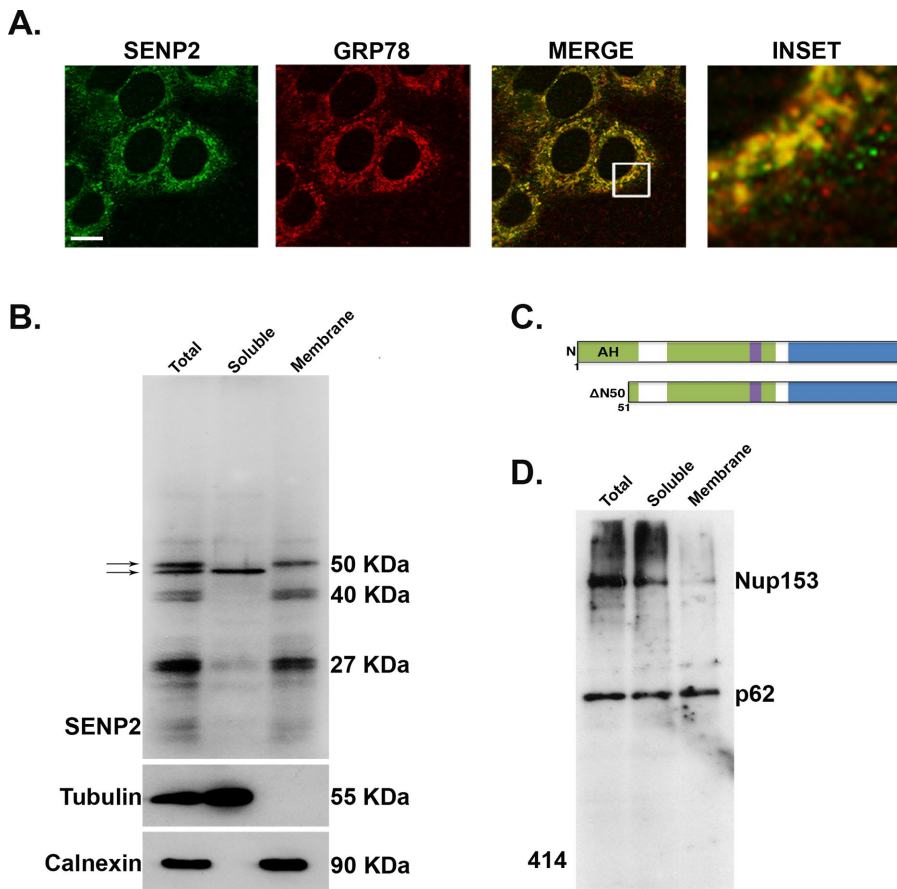


FIGURE 8: Endogenous SENP2 isoforms associate with intracellular membranes. (A) HeLa cells were fixed then permeabilized with digitonin. Cells were costained with anti-SENP2 and anti-GRP78 antibodies and then analyzed by indirect immunofluorescence microscopy. Endogenous SENP2 colocalized with GRP78, demonstrating ER membrane association. Scale bar = 5 μ m. (B) HeLa cells were fractionated by sucrose gradient sedimentation and fractions enriched in ER membranes were isolated and analyzed by immunoblotting. Anti-tubulin and anti-calnexin were used as markers for soluble and membrane fractions, respectively. SENP2 isoforms migrating at 50, 40, and 27 kDa were found in the membrane fraction. One of the two isoforms migrating at ~48 kDa, both indicated by black arrows, was present in the soluble fraction, suggesting the absence of the predicted amphipathic α -helix. (C) Schematic diagram representing the two potential SENP2 isoforms migrating at ~50 kDa, one lacking the first 50 amino acids. (D) Immunoblot using mAb414 showing the distribution of nucleoporins after HeLa cell fractionation. Nucleoporin p62 was equally distributed between the soluble and membrane fractions, while nucleoporin Nup153 was mostly soluble.

stretch of amino acids in their amphipathic α -helix (Nup1/Nup60 in yeast) have an important role in pore complex insertion into the nuclear membrane (Alber *et al.*, 2007; Doucet and Hetzer, 2010; Doucet *et al.*, 2010; Drin and Antonny, 2010; Meszaros *et al.*, 2015; Souquet and Doye, 2015). SENP2 has also been reported to play a role in NPC homeostasis, more specifically, when SENP1 and SENP2 are codepleted, the expression levels of certain nucleoporins decrease and are mislocalized (Chow *et al.*, 2014). Thus, it would be interesting to explore whether these effects are attributed to the ability of SENP2 to bind to membranes through its predicted amphipathic α -helix.

Another aspect of SENP2 that is shared with other proteins with amphipathic α -helices associated with the inner nuclear membrane, like yeast Nbp1 and Nup1/Nup60 (Nup153 in humans), is its ability to induce the formation of intranuclear membranes upon overexpression (Bastos *et al.*, 1996; Kupke *et al.*, 2011; Meszaros *et al.*, 2015). The overexpression of Nup1, for example, results in the de novo

synthesis of “expansion” membranes that are thought to arise as a secondary response to the physical stress imposed on the nuclear envelope (Meszaros *et al.*, 2015). We also noticed the formation of intranuclear membranes upon SENP2 overexpression, seen by immuno-EM as arrays of membranous structures. Although likely an artifact of overexpression, it is possible that the formation of intranuclear membranes is a product of a normal function of SENP2 amphipathic α -helix and its predicted ability to induce membrane curvature.

It is interesting to note that Nup1 overexpression results in the enlargement of cells indicating a mitotic defect, which was attributed to its amphipathic α -helix and its induction of membrane formation (Meszaros *et al.*, 2015). Similarly, it has been previously shown that SENP2 overexpression causes cell cycle arrest in mitosis (Zhang *et al.*, 2008). We asked whether this mitotic arrest is dependent on SENP2 amphipathic α -helix and induction of intranuclear membranes, and we found that the overexpression of either SENP2^{WT} or SENP2^{ΔN50} resulted in a similar mitotic phenotype (Supplemental Figure 5). Collectively, we found that the SENP2 predicted amphipathic α -helix shares many properties with amphipathic α -helices described for other proteins, suggesting important consequences for SENP2 function.

SENP2 and Kap- α regulation

Using *in vitro* and *in vivo* methods, we showed that the predicted amphipathic α -helix of SENP2 is regulated by its interactions with Kap- α . Kap- α binds to the NLS in close proximity to the amphipathic α -helix, thereby impeding interactions with cytoplasmic membranes. We propose that once SENP2 is transported into the nucleus and Kap- α is released, the helix is free to bind to the inner nuclear membrane, hence explaining the preferential localization of SENP2 (Figure 10).

Regulation of localization has been previously described for other proteins with predicted amphipathic α -helices and a proximal NLS, including Nbp1 (Kupke *et al.*, 2011), Nup60 (Meszaros *et al.*, 2015), Pom33 (Floch *et al.*, 2015), and Nup153 (Vollmer *et al.*, 2015). On the basis of our findings, we propose that karyopherin binding may serve as a common mechanism to regulate the relative distribution of these proteins between nuclear and cytoplasmic membranes.

Kap- α binding to SENP2 could be regulated at multiple levels. First, phosphorylation of SENP2 at amino acids within or in close proximity to the NLS could regulate the binding of Kap- α . Second, alternative splicing could result in protein variants lacking a functional NLS. Consistent with this latter mechanism, the bipartite NLS of SENP2 is split between two exons, exon 1 and exon 2. Collectively, either mechanism could explain our detection of endogenous SENP2 at both nuclear and cytoplasmic membranes.

It is also possible that alternative splicing could affect SENP2 localization by the presence or absence of the amphipathic α -helix

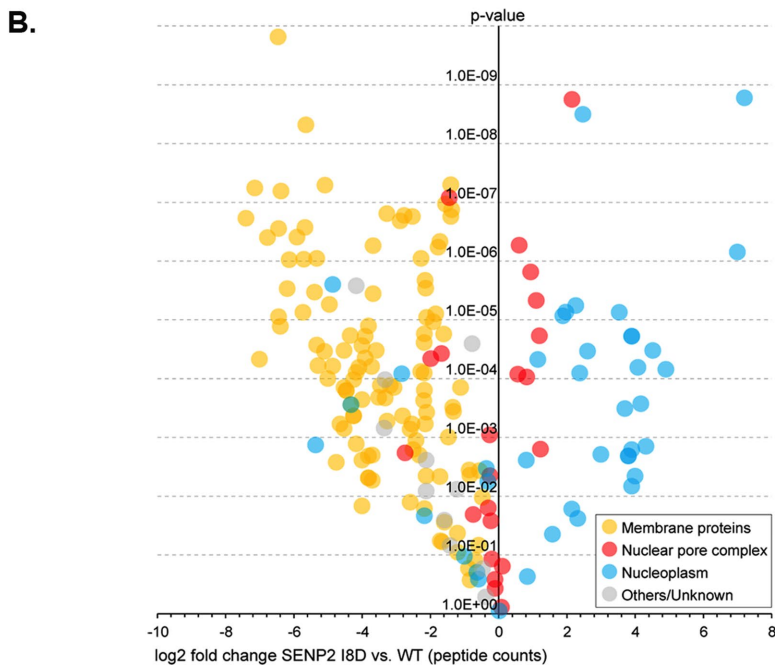
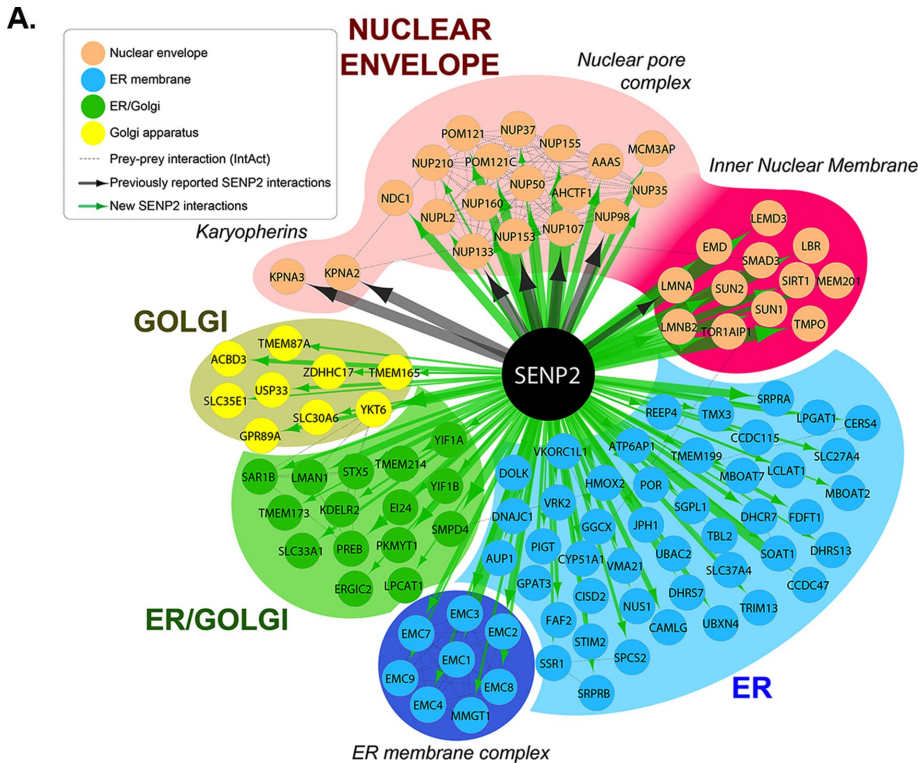


FIGURE 9: SENP2 interacts with ER, Golgi and inner nuclear membrane-associated proteins. SENP2^{WT} or SENP2^{I8D} fused to a promiscuous biotin ligase was stably expressed in 293 T-Rex Flp-In cells. Biotinylated proteins, comprising the pool of SENP2 interactors, were affinity purified using streptavidin and identified by mass spectrometry. (A) Schematic diagram showing SENP2^{WT} interactors. Black arrows indicate previously reported SENP2 interactions, and the green arrows indicate newly identified SENP2 interactions. Proteins were categorized into four broad categories: nuclear envelope (including karyopherins, nucleoporins, and inner nuclear membrane), ER membrane, ER/Golgi, and Golgi, indicated by pink, blue, green, and yellow circles, respectively. The complete list of BioID hits passing SAINT analysis (>0.75) is provided in Supplemental Table 1. (B) Volcano plot showing the log₂ fold change of protein hits identified to interact with SENP2^{WT} vs. those interacting with SENP2^{I8D}. Interactors were categorized into four different categories: membrane proteins, nuclear pore complex, nucleoplasm, and others/

itself. In fact, studies in mice have identified an alternatively spliced SENP2 variant lacking the first 50 N-terminal amino acids (Nishida et al., 2001). Consistently, we identified two SENP2 variants of ~50 and ~48 kDa that were detected in the membrane and soluble fractions, respectively (refer to Figure 8, B and C). Similarly to the SENP2 isoform identified in mice, we predict that the lower molecular weight variant lacks the amphipathic α -helix.

Sumoylation at intracellular membranes

Using BioID, we found that SENP2 interacts with a subset of membrane-associated proteins in the ER, Golgi, and inner nuclear membrane. These interactions are dependent on the presence of the predicted amphipathic α -helix. Notably, we did not capture those interactions in our previous AP-MS analysis (Goeres et al., 2011), likely reflecting the ability of BioID to more effectively capture dynamic, transient protein-protein interactions (Roux et al., 2013). Since proteins are covalently modified, harsher lysis methods can be employed enabling us to identify membrane or poorly soluble proteins. Additionally, weak interactors can be retained since protein-protein interactions do not have to be maintained postlysis (Coyaud et al., 2015). One caveat, however, is that the BioID does not differentiate between SENP2 substrates and interacting proteins. Nonetheless, the interacting proteins that were identified suggest new functions for sumoylation at membranes that must be further explored.

Closer analysis of the functions of the ER- and Golgi-associated proteins identified, we found that a significant number of these proteins are involved in vesicle-mediated transport, for example, YKT6, SAR1B, YIF1A, and PREB. Interestingly, studies in yeast also showed that SUMO interacts with a subset of proteins involved in vesicle transport, suggesting a role for sumoylation in regulating this process (Makhnevych et al., 2009). Taken together, we hypothesize that SENP2 may have a role in regulating vesicle-mediated transport by directly regulating the sumoylation of vesicle trafficking proteins.

unknown, indicated by yellow, red, blue, and gray circles, respectively. The *p* value was obtained from a *t* test comparing a series of four runs between the two baits (SENP2^{WT} and SENP2^{I8D}). SENP2^{I8D} lost association with multiple membrane proteins and gained new nucleoplasmic interactors. The complete list of protein hits is provided in Supplemental Table 2.

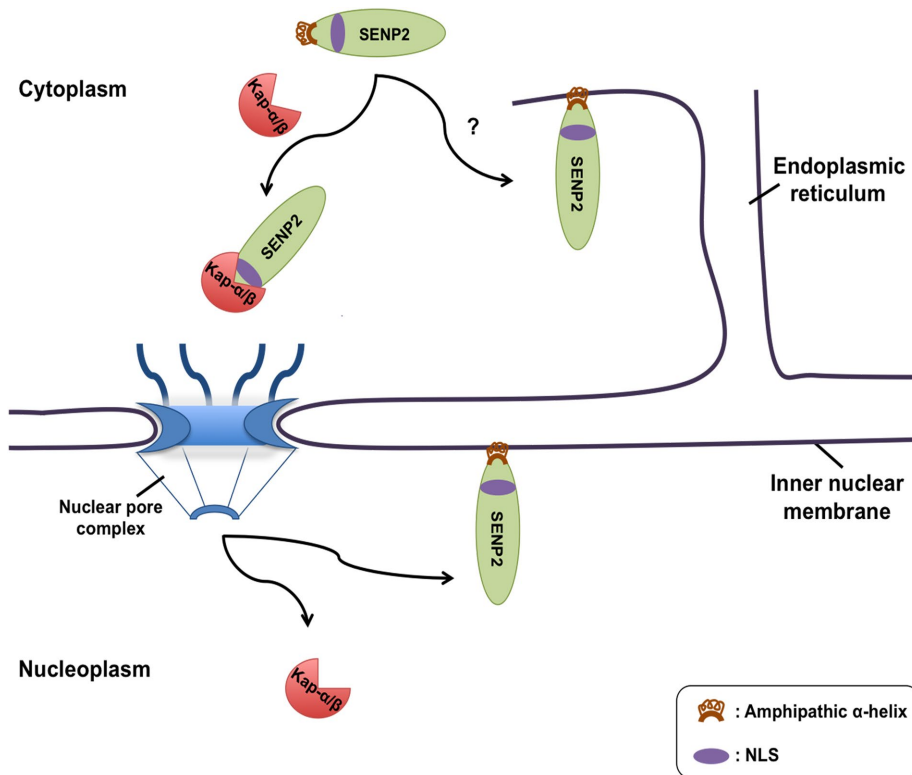


FIGURE 10: Schematic illustrating SENP2 membrane association and regulation by Kap- α binding. The binding of Kap- α to SENP2 impedes interactions with membranes in the cytoplasm. Following protein complex translocation to the nucleus via the import machinery Kap- α/β , Kap- α is released from SENP2, allowing the amphipathic α -helix to associate with the inner nuclear membrane. The binding of Kap- α to SENP2 may also be inhibited through unknown mechanisms (?) permitting the amphipathic α -helix to interact with the ER or Golgi membranes.

In addition to vesicle-mediated transport, sumoylation also plays a role in regulating the nuclear export and subsequent translation of mRNAs encoding secreted or membrane-targeted proteins. More specifically, a previous study showed that the SUMO E3 ligase, RanBP2/Nup358, located at the cytoplasmic face of the NPC, directly binds with the signal sequence coding regions of mRNAs, potentially coupling sumoylation with the biogenesis of membrane-targeted proteins (Mahadevan *et al.*, 2013). Given the interactions between SENP2 and ER-associated proteins, it will be valuable to explore the role of SENP2 in this process.

It is also worth noting that our BioID analysis identified multiple subunits of the ER membrane protein complex (EMC), including EMC1 through EMC5 (also known as MMEGT1), and EMC7-9 (refer to Figure 9A). EMC is a multifunctional 10-subunit protein complex involved in ER-associated degradation (ERAD), protein folding, cellular response to ER stress, lipid homeostasis, and the efficient insertion of tail-anchored proteins into ER membranes (Jonikas *et al.*, 2009; Christianson *et al.*, 2011; Richard *et al.*, 2013; Lahiri *et al.*, 2014; Satoh *et al.*, 2015; Wideman, 2015; Guna *et al.*, 2018). Since sumoylation is involved in regulating many of the same processes (Enserink, 2015), it is reasonable to suggest that SENP2 interaction with EMC subunits allows it to directly regulate those functions. It is also possible that the EMC complex itself may facilitate the binding of the SENP2 amphipathic α -helix to the ER membrane, but this requires further investigation.

Besides ER- and Golgi-associated proteins, a subset of proteins at the inner nuclear membrane was also found to interact with SENP2. Among those proteins, lamins stood out, as they are well-

studied SUMO substrates. Lamin A, for example, is known to be sumoylated at several lysine residues: K201, K420, and K486. Multiple mutations within the SUMO sites of lamin A result in decreased sumoylation and are associated with disease (laminopathies), more specifically, familial dilated cardiomyopathy or familial partial lipodystrophy (Zhang and Sarge, 2008; Simon *et al.*, 2013). How the sumoylation of lamin A is regulated is still unknown; however, based on the interactions we have identified between lamins and SENP2, we suggest that SENP2 may be playing a role in regulating the sumoylation process of lamins, particularly lamin A, and therefore regulating its functions.

In conclusion, our study opens doors to further explore the roles of sumoylation at membranes. As a crucial next step, SENP2 substrates, including potential candidates identified through BioID, need to be further characterized. Overall, our findings further illustrate the importance of the unique targeting signals in the N termini of SENPs and their role in defining localization and function. Additionally, based on Kap- α regulation of the amphipathic- α helix, we predict that the N-terminal signals themselves may be differentially regulated in response to the physiological needs of the cell.

MATERIALS AND METHODS

Antibodies

SENP2 and lamin B rabbit polyclonal antibodies were produced as previously described (Chaudhary and Courvalin, 1993; Goeres *et al.*, 2011). Remaining antibodies were obtained from the following sources: anti-GFP (Clontech, Mountain View, CA); anti-tubulin (Sigma-Aldrich, St. Louis, MO); anti-calnexin (Enzo Life Sciences, Farmingdale, NY); anti-MBP (GenScript, Piscataway, NJ); anti-FLAG M2 (Sigma-Aldrich); anti-His (Sigma-Aldrich, St. Louis, MO); anti-GM130 (BD Biosciences, San Jose, CA); anti-GRP78 (Santa Cruz Biotechnology, Dallas, TX); and mAb414 recognizing p62, Nup153, Nup214, and Nup358 (Abcam, Cambridge, MA).

Plasmid constructs

SENP2 cDNA was obtained as previously described (Zhang *et al.*, 2002). Full-length SENP2 and SENP2 deletion constructs (1-63, 143-350, and 10-63) were PCR amplified and cloned into pEGFP-C1 as described (Goeres *et al.*, 2011) and cloned into pEGFP-N1, using standard cloning procedures. SENP2 NLS mutation (R29A/R49A) and/or amphipathic α -helix mutation (I8D) were introduced using PCR-based, site-directed mutagenesis. SENP1 cDNA was a gift from Mary Dasso (National Institutes of Health, Bethesda, MD). Full-length SENP1 was cloned into pmCherry-C2 vector. MBP and MBP-SENP2 fusion proteins, SENP2(1-63)^{WT} and SENP2(1-63)^{I8D}, were cloned into a pRSF vector obtained from Jürgen Bosch (Johns Hopkins, Baltimore, MD) for bacterial expression. Kap- α_2 cDNA was obtained from a mouse fetal liver cDNA library and cloned into pET21a vector (EMD Biosciences, Gibbstown, NJ) as previously described (Goeres *et al.*, 2011).

Cell culture and transfection

HeLa cells were maintained in DMEM supplemented with 10% fetal bovine serum (FBS) at 37°C and 5% CO₂. Cells were grown at a confluency of 40–50% for transfection with the indicated plasmids using Lipofectamine 2000 according to manufacturer's protocol (Invitrogen, Carlsbad, CA). Cells were harvested either at 24 or 48 h posttransfection, as indicated, for immunoblotting or immunofluorescence microscopy.

Immunoblotting

Immunoblot analysis was performed either using enzyme-linked chemiluminescence ECL-Prime reagent (GE Healthcare, Silver Spring, MD) and developed with film or using IRDye-conjugated secondary antibodies and imaged using Odyssey infrared imager (LI-COR).

Immunofluorescence microscopy

HeLa cells were cultured on glass coverslips. Cells were fixed with 2% formaldehyde in 1X phosphate-buffered saline (PBS) for 30 min at room temperature, and then permeabilized in 0.2% Triton X-100 in 1X PBS for 6 min at room temperature. Immunostaining was carried out as previously described (Matunis *et al.*, 1996). For ER and Golgi staining, cells were fixed as described above, and then permeabilized using 0.05% digitonin for 6 min. Zeiss Observer Z1 fluorescence microscope with an Apotome V_H optical sectioning grid (Cal Zeiss, Jena, Germany) was used to acquire images.

Immunolectron microscopy

HeLa cells were processed for indirect immunolabeling of ultrathin cryosections essentially as previously described (McCaffery and Farquhar, 1995). Briefly, cells were fixed in a monolayer at 4°C in 100 mM PO₄ (pH 7.4) and 2.5% sucrose and containing 4% formaldehyde. The cells were harvested, pelleted, and cryo-protected in 2.3 M sucrose containing 30% polyvinyl pyrrolidone. Cell pellets were mounted onto aluminum cryopins and frozen in liquid nitrogen. Ultrathin cryosections were then cut on a Leica UCT ultramicrotome equipped with a fetal calf serum (FCS) cryostage, and sections were collected onto 300 mesh, formvar/carbon-coated nickel grids. Grids were washed, blocked in 10% FCS, and incubated overnight with primary chicken anti-GFP antibody (10 µg/ml). After being washed, grids were incubated with 6- or 12-nm Au-conjugated donkey anti-chicken antibody (Jackson ImmunoResearch Labs, Ft. Washington, PA) for 2 h, washed, and subsequently embedded in a mixture containing 3.2% polyvinyl alcohol (10,000 MW), 0.2% methyl cellulose (400 centipoises), and 0.2% uranyl acetate. Sections were analyzed on a Tecnai 12 transmission electron microscope and images collected with a Soft Imaging System Megaview III digital camera.

Recombinant protein expression and purification

MBP-tagged SENP2(1-63)^{WT}, SENP2(1-63)^{BD}, or MBP construct alone were transformed into *Escherichia coli* Rosetta competent cells. Expression was induced using 0.5 mM isopropylthiogalactoside (IPTG) at 20°C overnight. Cells were pelleted and resuspended in ice-cold lysis buffer (50 mM Tris-HCl [pH 7.5], 150 mM NaCl, 1 mM EDTA, 1 mM phenylmethylsulfonyl fluoride [PMSF], 5 mg/ml leupeptin and pepstatin A, 1 mM dithiothreitol [DTT], and 1 mg/ml lysozyme). Suspensions were sonicated for a total of 1 min, 0.5-s intervals, and then centrifuged at 30,000 × *g* for 30 min at 4°C. The supernatant was incubated with equilibrated amylose resin (New England Biolabs, Ipswich, MA) for 2 h at 4°C with end-to-end rotation. Bound protein was eluted in buffer containing 50 mM Tris-HCl (pH 7.5), 150 mM NaCl, 1 mM EDTA, 1 mM DTT, and 20 mM maltose.

His-tagged mouse Kap-α₂ was expressed in *E. coli* Rosetta competent cells as described above and purified using Ni-NTA agarose affinity column chromatography, according to manufacturer's protocol (Qiagen). For expression and purification of MBP-SENP2(1-63)^{WT} in complex with His-tagged Kap-α₂, both protein expression constructs were cotransformed in *E. coli* Rosetta competent cells. Coexpression was induced using 0.5 mM IPTG at 20°C overnight. Complex purification was performed as described above. A final concentration of 20 mM maltose was added to coelute the protein complex.

In vitro liposome cosedimentation assay

Lipids dissolved in chloroform, purchased from Avanti Polar Lipids (Alabaster, AL), were mixed together in a glass tube to make the following lipid composition: 79 mol% phosphatidylcholine (PC), 20 mol% phosphatidylethanolamine (PE), and 1 mol% NBD-labeled phosphatidylethanolamine (NBD-PE). Lipid vesicles were prepared essentially as previously described (Tu-Sekine and Raben, 2012). Briefly, the homogeneous lipid mixture was dried under dry nitrogen stream and stored under vacuum for 2–20 h to remove residual chloroform. Lipid films were rehydrated with hydration buffer (50 mM Tris-HCl [pH 7.5], 150 mM NaCl, 1 mM EDTA, and 176 mM sucrose) at 37°C for 30 min. During hydration, and in 10-min intervals, samples were vortexed and then sonicated in a water bath sonicator for 30 s until the lipid films were completely resuspended. Vesicles were formed by extrusion through a 100-nm polycarbonate membrane, using an Avanti mini-extruder and following manufacturer's protocol. Sucrose-filled liposomes were then diluted with binding buffer (50 mM Tris-HCl [pH 7.5], 150 mM NaCl, and 1 mM EDTA) at a 1:4 ratio and then spun down at 186,000 × *g* in a tabletop ultracentrifuge at 22°C for 1 h. Pellets were resuspended with binding buffer and concentrations were determined using a spectrophotometer. A fresh liposomes batch was prepared for each experiment. For liposome cosedimentation assays, 1.5, 3, 6, or 12 mM liposomes were mixed with 0.7 µg of protein prepared in binding buffer, in a total volume of 100 µl per reaction. Liposomes and protein were incubated for 30 min at room temperature. The reaction was pelleted at 186,000 × *g* in a tabletop ultracentrifuge at 22°C for 1 h. Equal volumes of pellet and supernatant were analyzed by SDS-PAGE, followed by immunoblotting. It should be noted that apparent maximal protein binding varied between individual experiments but that variability within experimental replicates was low.

Subcellular fractionation

Isolation of ER membranes was performed as previously described (Bozidis *et al.*, 2007). Briefly, HeLa cells were seeded in 55-cm² plates and either untreated or transfected with GFP-SENP2(1-63)^{mNLS} or GFP-SENP2(1-63)^{mNLS/BD}. After 24 h, cells were harvested and pelleted by centrifugation at 200 × *g* for 10 min at 4°C. Cells were lysed in 1X MTE buffer (270 mM d-mannitol, 10 mM Tris-base [pH 7.4], 0.1 mM EDTA). Lysate was sonicated for a total of 30 s, 10-s intervals, and then centrifuged at 1400 × *g* for 15 min at 4°C. To separate crude ER from crude mitochondria, supernatant was centrifuged at 15,000 × *g* for 15 min. To purify ER membranes, supernatant was layered on top of a discontinuous sucrose gradient (from bottom to top: 2 ml of 2.0 M sucrose, 3 ml of 1.5 M sucrose, 3 ml of 1.3 M sucrose) in a polyallomer ultracentrifuge tube (Beckman Coulter, Indianapolis, IN). ER sucrose gradients were centrifuged for 70 min at 152,000 × *g*. Banded ER membranes at the 1.3 M sucrose interface were collected using an 18-gauge needle and then transferred to a new polyallomer tube and pelleted at 126,000 × *g* for 45 min. Pellets containing ER membranes were resuspended in 1X

MTE buffer. Fractions collected were analyzed by SDS–PAGE followed by immunoblotting.

Stable cell lines and biotin-streptavidin affinity purification for BioID

Stable cell lines for BioID analysis were established essentially as previously described (Gupta *et al.*, 2015). In brief, the full-length human SENP2 (BC040609) coding sequence was amplified by PCR and cloned into pcDNA5 FRT/TO FLAG-BirA* expression vector. Using the Flp-In system (Invitrogen, Carlsbad, CA), 293 T-REx Flp-In cells stably expressing FLAG-BirA* alone, FLAG-BirA*-SENP2^{WT}, or FLAG-BirA*-SENP2^{BD} were generated. Plates (10 × 150 cm²) of subconfluent (60%) cells were incubated for 24 h in complete media supplemented with 1 µg/ml tetracycline (Sigma-Aldrich) and 50 µM biotin (BioShop Canada, Ontario, Canada). Cells were collected and pelleted (200 × g, for 3 min), the pellet was washed twice with PBS, and dried pellets were snap frozen.

Cell pellets were resuspended in 10 ml of lysis buffer (50 mM Tris-HCl [pH 7.5], 150 mM NaCl, 1 mM EDTA, 1 mM egtazic acid [EGTA], 1% Triton X-100, 0.1% SDS, 1:500 protease inhibitor cocktail [Sigma-Aldrich], 1:1000 benzonase nuclease [Novagen]) and incubated on an end-to-end rotator at 4°C for 1 h, briefly sonicated to disrupt any visible aggregates, and then centrifuged at 45,000 × g for 30 min at 4°C. Supernatant was transferred to a fresh 15 ml conical tube. Packed, pre-equilibrated streptavidin sepharose beads (30 µl) (GE Healthcare, Silver Spring, MD) were added, and the mixture was incubated for 3 h at 4°C with end-to-end rotation. Beads were pelleted by centrifugation at 2000 × g for 2 min and transferred with 1 ml of lysis buffer to a fresh microcentrifuge tube. Beads were washed once with 1 ml lysis buffer and twice with 1 ml of 50 mM ammonium bicarbonate (pH 8.3). Beads were transferred in ammonium bicarbonate to a fresh centrifuge tube and washed two more times with 1 ml ammonium bicarbonate buffer. Tryptic digestion was performed by incubating the beads with 1 µg MS-grade *N*-tosyl-L-phenylalanine chloromethyl ketone (TPCK) trypsin (Promega, Madison, WI) dissolved in 200 µl of 50 mM ammonium bicarbonate (pH 8.3) overnight at 37°C. The following morning, 0.5 µg MS-grade TPCK trypsin was added, and beads were incubated 2 additional hours at 37°C. Beads were pelleted by centrifugation at 2000 × g for 2 min, and the supernatant was transferred to a fresh microcentrifuge tube. Beads were washed twice with 150 µl of 50 mM ammonium bicarbonate, and washes were pooled with the eluate. The sample was lyophilized and resuspended in buffer A (0.1% formic acid). One-fifth of the sample was analyzed per MS run.

Mass spectrometry

Analytical columns (75 µm inner diameter) and precolumns (150 µm inner diameter) were made in-house from fused silica capillary tubing from InnovaQuartz (Phoenix, AZ) and packed with 100-Å C18-coated silica particles (Magic, Michrom Bioresources, Auburn, CA). Peptides were subjected to liquid chromatography (LC)-electrospray ionization-tandem mass spectrometry, using a 120-min reversed-phase (100% water–100% acetonitrile, 0.1% formic acid) buffer gradient running at 250 ml/min on a Proxeon EASY-nLC pump in-line with a hybrid linear trap quadrupole (LTQ)-Orbitrap Velos mass spectrometer (Thermo Fisher Scientific, Waltham, MA). A parent ion scan was performed in the Orbitrap using a resolving power of 60,000, and then up to the 20 most intense peaks were selected for MS/MS (minimum ion count of 1000 for activation), using standard collision induced dissociation fragmentation. Fragment ions were detected in the LTQ. Dynamic exclusion was activated such that MS/MS of the same *m/z* (within a range of 15 ppm;

exclusion list size = 500) detected twice within 15 s were excluded from analysis for 30 s. For protein identification, Thermo .RAW files were converted to .mzXML format using Proteowizard (Kessner *et al.*, 2008) and then searched using X!Tandem (Craig and Beavis, 2004) against the human (Human RefSeq Version 45) database. X!Tandem search parameters were as follows: 15ppm parent mass error; 0.4 Da fragment mass error; complete modifications, none; cysteine modifications, none; potential modifications, +16@M and W, +32@M and W, +42@N-terminus, +1@N and Q. Data were analyzed using the transproteomic pipeline (Deutsch *et al.*, 2010; Pedrioli, 2010) via the ProHits software suite (Liu *et al.*, 2010). Proteins identified with a Protein Prophet cutoff of 0.9 and at least two unique peptides were analyzed with the SAINT express algorithm (v3.6.1) (Teo *et al.*, 2014). Sixteen control runs (consisting of 12 FLAG-BirA* only and four samples with no bait expressed) were collapsed to the two highest spectral counts for each prey, and the SAINT score cutoff value was set to a Bayesian false discovery rate (BFDR) < 0.01 (1% false discovery rate [FDR]). A network of high confidence interactors was assembled using Cytoscape (3.4.0).

ACKNOWLEDGMENTS

We thank all the members of the Matunis lab for helpful advice and support during the course of this work. We also thank Daniel Raben and Becky Tu-Sekine (Johns Hopkins University, Baltimore, MD) for their generous support and advice on preparing and analyzing synthetic liposomes. We thank Carolyn Machamer (Johns Hopkins University, Baltimore, MD) for providing us with the ER and Golgi antibodies and for her invaluable input on staining cells for indirect immunofluorescence microscopy. We also acknowledge the technical assistance and expertise of the Integrated Imaging Center at the Johns Hopkins University for the immunoelectron microscopy and National Institutes of Health National Center for Research Resources grant 1S10RR023454-01 awarded to J. Michael McCaffery. This work was supported by a grant from the National Institutes of Health (GM060890 to M.J.M.) and the Canadian Institutes of Health Research (MOP130340 to B.R.).

REFERENCES

- Alber F, Dokudovskaya S, Veenhoff LM, Zhang W, Kipper J, Devos D, Suprpto A, Karni-Schmidt O, Williams R, Chait BT, *et al.* (2007). The molecular architecture of the nuclear pore complex. *Nature* 450, 695–701.
- Anderson CA, Blackstone C (2013). SUMO wrestling with Drp1 at mitochondria. *EMBO J* 32, 1496–1498.
- Bastos R, Lin A, Enarson M, Burke B (1996). Targeting and function in mRNA export of nuclear pore complex protein Nup153. *J Cell Biol* 134, 1141–1156.
- Bozidis P, Williamson CD, Colberg-Poley AM (2007). Isolation of endoplasmic reticulum, mitochondria, and mitochondria-associated membrane fractions from transfected cells and from human cytomegalovirus-infected primary fibroblasts. *Curr Protoc Cell Biol* Chapter 3, Unit 3.27.
- Cappadocia L, Lima CD (2018). Ubiquitin-like protein conjugation: structures, chemistry, and mechanism. *Chem Rev* 118, 889–918.
- Chaudhary N, Courvalin JC (1993). Stepwise reassembly of the nuclear envelope at the end of mitosis. *J Cell Biol* 122, 295–306.
- Choi H, Liu G, Mellacheruvu D, Tyers M, Gingras AC, Nesvizhskii AI (2012). Analyzing protein-protein interactions from affinity purification-mass spectrometry data with SAINT. *Curr Protoc Bioinformatics* Chapter 8, Unit 8.15.
- Chow KH, Elgort S, Dasso M, Powers MA, Ullman KS (2014). The SUMO proteases SENP1 and SENP2 play a critical role in nucleoporin homeostasis and nuclear pore complex function. *Mol Biol Cell* 25, 160–168.
- Chow KH, Elgort S, Dasso M, Ullman KS (2012). Two distinct sites in Nup153 mediate interaction with the SUMO proteases SENP1 and SENP2. *Nucleus* 3, 349–358.
- Christianson JC, Olzmann JA, Shaler TA, Sowa ME, Bennett EJ, Richter CM, Tyler RE, Greenblatt EJ, Harper JW, Kopito RR (2011). Defining human

- ERAD networks through an integrative mapping strategy. *Nat Cell Biol* 14, 93–105.
- Citro S, Cicocca S (2013). Sumo paralogs: redundancy and divergencies. *Front Biosci* 5, 544–553.
- Coyaud E, Mis M, Laurent EM, Dunham WH, Couzens AL, Robitaille M, Gingras AC, Angers S, Raught B (2015). BioID-based identification of Skp cullin F-box (SCF) β -TrCP1/2 E3 ligase substrates. *Mol Cell Proteomics* 14, 1781–1795.
- Craig R, Beavis RC (2004). TANDEM: matching proteins with tandem mass spectra. *Bioinformatics* 20, 1466–1467.
- Cubeñas-Potts C, Goeres JD, Matunis MJ (2013). SENP1 and SENP2 affect spatial and temporal control of sumoylation in mitosis. *Mol Biol Cell* 24, 3483–3495.
- Deutsch EW, Mendoza L, Shteynberg D, Farrah T, Lam H, Tasman N, Sun Z, Nilsson E, Pratt B, Prazen B, et al. (2010). A guided tour of the trans-proteomic pipeline. *Proteomics* 10, 1150–1159.
- Doucet CM, Hetzer MW (2010). Nuclear pore biogenesis into an intact nuclear envelope. *Chromosoma* 119, 469–477.
- Doucet CM, Talamas JA, Hetzer MW (2010). Cell cycle-dependent differences in nuclear pore complex assembly in metazoa. *Cell* 141, 1030–1041.
- Drin G, Antonny B (2010). Amphipathic helices and membrane curvature. *FEBS Lett* 584, 1840–1847.
- Drin G, Casella JF, Gautier R, Boehmer T, Schwartz TU, Antonny B (2007). A general amphipathic alpha-helical motif for sensing membrane curvature. *Nat Struct Mol Biol* 14, 138–146.
- Enserink JM (2015). Sumo and the cellular stress response. *Cell Div* 10, 4.
- Floch AG, Taresté D, Fuchs PF, Chadrin A, Naciri I, Leger T, Schlenstedt G, Palancade B, Doye V (2015). Nuclear pore targeting of the yeast Pom33 nucleoporin depends on karyopherin and lipid binding. *J Cell Sci* 128, 305–316.
- Fu J, Yu HM, Chiu SY, Mirando AJ, Maruyama EO, Cheng JG, Hsu W (2014). Disruption of SUMO-specific protease 2 induces mitochondria mediated neurodegeneration. *PLoS Genet* 10, e1004579.
- Goeres J, Chan PK, Mukhopadhyay D, Zhang H, Raught B, Matunis MJ (2011). The SUMO-specific isopeptidase SENP2 associates dynamically with nuclear pore complexes through interactions with karyopherins and the Nup107–160 nucleoporin subcomplex. *Mol Biol Cell* 22, 4868–4882.
- Gong X, Ahner A, Roldan A, Lukacs GL, Thibodeau PH, Frizzell RA (2016). Non-native conformers of cystic fibrosis transmembrane conductance regulator NBD1 are recognized by Hsp27 and conjugated to SUMO-2 for degradation. *J Biol Chem* 291, 2004–2017.
- Guna A, Volkmar N, Christianson JC, Hegde RS (2018). The ER membrane protein complex is a transmembrane domain insertase. *Science* 359, 470–473.
- Gupta GD, Coyaud E, Goncalves J, Mojarad BA, Liu Y, Wu Q, Gheiratmand L, Comartin D, Tkach JM, Cheung SW, et al. (2015). A dynamic protein interaction landscape of the human centrosome-cilium interface. *Cell* 163, 1484–1499.
- Hang J, Dasso M (2002). Association of the human SUMO-1 protease SENP2 with the nuclear pore. *J Biol Chem* 277, 19961–19966.
- Hay RT (2013). Decoding the SUMO signal. *Biochem Soc Trans* 41, 463–473.
- Hendriks IA, Vertegaal AC (2016). A comprehensive compilation of SUMO proteomics. *Nat Rev Mol Cell Biol* 17, 581–595.
- Hickey CM, Wilson NR, Hochstrasser M (2012). Function and regulation of SUMO proteases. *Nat Rev Mol Cell Biol* 13, 755–766.
- Itahana Y, Yeh ET, Zhang Y (2006). Nucleocytoplasmic shuttling modulates activity and ubiquitination-dependent turnover of SUMO-specific protease 2. *Mol Cell Biol* 26, 4675–4689.
- Jonikas MC, Collins SR, Denic V, Oh E, Quan EM, Schmid V, Weibezahn J, Schwappach B, Walter P, Weissman JS, Schuldiner M (2009). Comprehensive characterization of genes required for protein folding in the endoplasmic reticulum. *Science* 323, 1693–1697.
- Kessner D, Chambers M, Burke R, Agus D, Mallick P (2008). ProteoWizard: open source software for rapid proteomics tools development. *Bioinformatics* 24, 2534–2536.
- Kupke T, Di Cecco L, Muller HM, Neuner A, Adolf F, Wieland F, Nickel W, Schiebel E (2011). Targeting of Nbp1 to the inner nuclear membrane is essential for spindle pole body duplication. *EMBO J* 30, 3337–3352.
- Lahiri S, Chao JT, Tavassoli S, Wong AK, Choudhary V, Young BP, Loewen CJ, Prinz WA (2014). A conserved endoplasmic reticulum membrane protein complex (EMC) facilitates phospholipid transfer from the ER to mitochondria. *PLoS Biol* 12, e1001969.
- Liu G, Zhang J, Larsen B, Stark C, Breitkreutz A, Lin ZY, Breitkreutz BJ, Ding Y, Colwill K, Pasculescu A, et al. (2010). ProHits: integrated software for mass spectrometry-based interaction proteomics. *Nat Biotechnol* 28, 1015–1017.
- Mahadevan K, Zhang H, Akef A, Cui XA, Gueroussov S, Cenik C, Roth FP, Palazzo AF (2013). RanBP2/Nup358 potentiates the translation of a subset of mRNAs encoding secretory proteins. *PLoS Biol* 11, e1001545.
- Makhnevych T, Sydorsky Y, Xin X, Srikumar T, Vizeacoumar FJ, Jeram SM, Li Z, Bahr S, Andrews BJ, Boone C, Raught B (2009). Global map of SUMO function revealed by protein-protein interaction and genetic networks. *Mol Cell* 33, 124–135.
- Matunis MJ, Coutavas E, Blobel G (1996). A novel ubiquitin-like modification modulates the partitioning of the Ran-GTPase-activating protein RanGAP1 between the cytosol and the nuclear pore complex. *J Cell Biol* 135, 1457–1470.
- McCaffery JM, Farquhar MG (1995). Localization of GTPases by indirect immunofluorescence and immunoelectron microscopy. *Methods Enzymol* 257, 259–279.
- Meng X, Clews J, Kargas V, Wang X, Ford RC (2017). The cystic fibrosis transmembrane conductance regulator (CFTR) and its stability. *Cell Mol Life Sci* 74, 23–38.
- Meszáros N, Cibulka J, Mendiburo MJ, Romanauska A, Schneider M, Kohler A (2015). Nuclear pore basket proteins are tethered to the nuclear envelope and can regulate membrane curvature. *Dev Cell* 33, 285–298.
- Nayak A, Muller S (2014). SUMO-specific proteases/isopeptidases: SENPs and beyond. *Genome Biol* 15, 422.
- Nishida T, Kaneko F, Kitagawa M, Yasuda H (2001). Characterization of a novel mammalian SUMO-1/Smt3-specific isopeptidase, a homologue of rat axam, which is an axin-binding protein promoting beta-catenin degradation. *J Biol Chem* 276, 39060–39066.
- Pedrioli PG (2010). Trans-proteomic pipeline: a pipeline for proteomic analysis. *Methods Mol Biol* 604, 213–238.
- Qi Y, Wang J, Bomben VC, Li DP, Chen SR, Sun H, Xi Y, Reed JG, Cheng J, Pan HL, et al. (2014). Hyper-SUMOylation of the Kv7 potassium channel diminishes the M-current leading to seizures and sudden death. *Neuron* 83, 1159–1171.
- Richard M, Boulin T, Robert VJ, Richmond JE, Bessereau JL (2013). Biosynthesis of ionotropic acetylcholine receptors requires the evolutionarily conserved ER membrane complex. *Proc Natl Acad Sci USA* 110, E1055–E1063.
- Roux KJ, Kim DI, Burke B (2013). BioID: a screen for protein-protein interactions. *Curr Protoc Protein Sci* 74, Unit 19 23.
- Sapay N, Guermeur Y, Deleage G (2006). Prediction of amphipathic in-plane membrane anchors in monotopic proteins using a SVM classifier. *BMC Bioinform* 7, 255.
- Satoh T, Ohba A, Liu Z, Inagaki T, Satoh AK (2015). dPob/EMC is essential for biosynthesis of rhodopsin and other multi-pass membrane proteins in *Drosophila* photoreceptors. *eLife* 4, e06306.
- Simon DN, Domaradzki T, Hofmann WA, Wilson KL (2013). Lamin A tail modification by SUMO1 is disrupted by familial partial lipodystrophy-causing mutations. *Mol Biol Cell* 24, 342–350.
- Souquet B, Doye V (2015). Bending or building: multifaceted functions of amphipathic helices in basket nucleoporins. *Dev Cell* 33, 626–628.
- Teo G, Liu G, Zhang J, Nesvizhskii AI, Gingras AC, Choi H (2014). SAINTexpress: improvements and additional features in Significance Analysis of INTERactome software. *J Proteomics* 100, 37–43.
- Tu-Sekine B, Raben DM (2012). Dual regulation of diacylglycerol kinase (DGK)-theta: polybasic proteins promote activation by phospholipids and increase substrate affinity. *J Biol Chem* 287, 41619–41627.
- Vollmer B, Lorenz M, Moreno-Andres D, Bodenhofer M, De Magistris P, Astrinidis SA, Schooley A, Flotenmeyer M, Leptihn S, Antonin W (2015). Nup153 recruits the Nup107–160 complex to the inner nuclear membrane for interphasic nuclear pore complex assembly. *Dev Cell* 33, 717–728.
- Wasik U, Filipek A (2014). Non-nuclear function of sumoylated proteins. *Biochim Biophys Acta* 1843, 2878–2885.
- Wideman JG (2015). The ubiquitous and ancient ER membrane protein complex (EMC): tether or not? *F1000Research* 4, 624.
- Wilson VG (2017). Introduction to Sumoylation. *Adv Exp Med Biol* 963, 1–12.
- Zhang H, Saitoh H, Matunis MJ (2002). Enzymes of the SUMO modification pathway localize to filaments of the nuclear pore complex. *Mol Cell Biol* 22, 6498–6508.
- Zhang XD, Goeres J, Zhang H, Yen TJ, Porter AC, Matunis MJ (2008). SUMO-2/3 modification and binding regulate the association of CENP-E with kinetochores and progression through mitosis. *Mol Cell* 29, 729–741.
- Zhang YQ, Sarge KD (2008). Sumoylation regulates lamin A function and is lost in lamin A mutants associated with familial cardiomyopathies. *J Cell Biol* 182, 35–39.